sciendo

Green Sciences, 27, 2, 17—27, 10.2478/pjct-2025-0009

Development and properties of cementitious self-healing materials based on composite complexing agents

Hongjie Li[1], Yanbao Liu[2,3,*], Quanbin Ba[2,3]

[1]Division of Logistics and Infrastructure, Sichuan International Studies University, Chongqing, 400031, China
[2]State Key Laboratory of Coal Mine Disaster Prevention and Control, Chongqing 400037, China
[3]CCTEG Chongqing Research Institute, Chongqing 400039, China
[*]*Corresponding author:* e-mail: yanbao_liu@163.com

In addressing the concerns regarding structural performance degradation and diminished service life resulting from concrete crack formation during utilization, this study has developed a cement-based self-healing material. This material utilizes a composite complexing agent composed of tartaric acid derivatives, sodium hexametaphosphate, ethylenediaminetetraacetic acid tetrasodium salt, and vinyl acetate-ethylene redispersible latex powder. The material composition was optimized, and its self-healing performance and mechanism were systematically studied. The findings indicated that when the composite complexing agent content was set at 6% by mass of cement, there was a substantial decrease in the porosity, from 34.2% to 14.2%. In comparison with the control group, specimens with a 6% composite complexing agent exhibited an 8.3 MPa increase in compressive strength and a substantial enhancement in crack sealing, with a rate increase from 73.1% to 99.7%, following 28 days of water curing.

Keywords: Composite Complexing Agent; Cement-Based Materials; Self-Healing Mechanism; Performance Study.

Received: 14 January 2025; Accepted: 23 March 2025; Available online: 28.07.2025.

INTRODUCTION

Concrete, a pivotal material in contemporary construction, finds extensive application in various infrastructure and building projects[1]. However, it is susceptible to crack formation under the influence of multifaceted factors, including external loads and environmental erosion. These cracks permit the intrusion of harmful substances, such as water, chloride ions, and sulfates, which can lead to a reduction in concrete strength, durability, and permeability, thus compromising its ability to meet engineering requirements[2–4]. Consequently, crack repair has emerged as the predominant approach to address the durability concerns of concrete[5, 6]. However, conventional repair methodologies encounter challenges such as substantial expenses, intricate procedures, and challenges in specific application scenarios. Therefore, enhancing concrete's inherent capacity for spontaneous crack repair has been demonstrated to reduce maintenance expenditures and significantly extend the service life of concrete structures. This has emerged as a pivotal research direction in concrete technology in recent years.

The study of concrete crack self-repair involves a variety of techniques, including electrodeposition[7], capsule-based self-healing[8–10], magnesium oxide expansive agent self-healing[11–13], shape memory alloy self--healing[14–16], fiber-reinforced concrete self-healing[17, 18], biologically-inspired self-healing[19, 20], and permeability crystallization-based self-healing technology[21, 22]. Among them, the permeability crystallization technology began in 1942 with the development of permeability crystallization materials by German chemist Lauritz Jensen[23]. By adding specific chemical components to concrete, these materials can penetrate into crack regions when cracks form, stimulating unhydrated cement particles to undergo further hydration reactions, thereby achieving automatic crack repair. In recent years, this technology has received widespread attention and in-depth research. Ren et al.[24] demonstrated in their study that crystalline additives effectively improved the concrete's pore structure and minimized its porosity. Zhang[25] investigated the effects of four ionic complexing agents, including sodium hexametaphosphate, polyaminocarboxylate tetrasodium, ethylenediaminetetraacetic acid tetrasodium, and diethylene triamine pentaacetic acid pentasodium, and explored the promoting effect of calcium formate on crack self-healing performance. Xia et al.[26] investigated the role of complexing agents, including tartaric acid derivatives, in enhancing the self-repairing properties of cracks. They analyzed the mechanisms behind the effectiveness of these agents. Zhang et al.[27] investigated the influence mechanism of various ion chelators on the mechanical, transport, and microstructure properties of cement-based materials.

In this study, a composite complexing agent based on tartaric acid derivatives, sodium hexametaphosphate, and ethylenediaminetetraacetic acid tetrasodium salt was developed as the core component of self-healing materials. The optimal formulation of the complexing agent was determined by orthogonal experiments, and its effect on the pore characteristics and fundamental properties of the cement paste was systematically evaluated by mercury intrusion porosimetry and thermal analysis. Then, the application effect of the composite complexing agent in crack self-healing was verified by compressive strength experiments and permeability tests. Finally, the types of products generated in the crack region and their repair mechanisms were analyzed using X-ray diffraction technology. The objective of this study is to provide a theoretical and experimental basis for the use of composite complexing agents in the self-healing technology of cement-based materials.

MATERIALS AND METHODS

Experimental Materials and Formulations

Raw Materials

The following substances are considered the primary raw materials: ordinary Portland cement, deionized water, tartaric acid derivatives (DPA), sodium hexametaphosphate (SHMP), ethylenediaminetetraacetic acid tetrasodium salt (EDTA-4Na), vinyl acetate-ethylene (VAE) redispersible latex powder, fly ash, water reducers, retarders, and other admixtures.

Cement, the main component of the self-healing material, was sourced from Jiahua Special Cement Co., Ltd. The composition is provided in Table 1.

Sodium hexametaphosphate, ethylenediaminetetraacetic acid tetrasodium salt, and redispersible latex powder were selected from Shandong Yousuo Chemical Co., Ltd., and are analytical-grade reagents.

Tartaric acid derivatives were selected from Wuhan Xinwei Welding Chemical Co., Ltd., and are analytical--grade reagents.

The fly ash composition is shown in Table 2.

Specimen Preparation Method

(1) Preparation of DPA Reagent

In this study, a water-soluble polymerization method was used to polymerize the carbon-carbon double bonds in DPA. Although the resulting polymer is a low molecular weight substance, its unique spatial configuration effectively protects the carboxyl group (-COOH) and prevents it from prematurely participating in reactions.

During the initial mixing of the cement, the steric hindrance effect of the DPA polymer can moderately regulate the chelation between the carboxyl group and calcium ions, preventing excessive chelation that could lead to retarded setting. This ensures normal setting and hardening of the cement paste. As the cement system sets and the environment becomes highly alkaline, it promotes controlled hydrolysis of the DPA polymer. The hydrolysis products exhibit delayed activity, allowing them to quickly migrate to microcracks and participate in reactions. The development of novel hydration products that bridge these cracks has been shown to significantly increase the concrete's ability to self-heal and improve its long-term durability.

Reagent Preparation Method:

1. Dissolution and Dispersion

Weigh a certain amount of DPA into a three-necked flask and add deionized water. Heat and stir using a magnetic stirrer to ensure that the DPA is completely dissolved and uniformly dispersed. The flask is equipped with a condenser, a nitrogen inlet tube, and a magnetic stirrer. The condenser controls the temperature, the nitrogen inlet maintains an anaerobic environment to prevent oxidation, and the stirrer maintains the uniformity of the solution.

2. Initiator Solution Preparation

Weigh ammonium persulfate (APS) and sodium bisulfite (SBS) at room temperature, dissolve in deionized water, and prepare the initiator solution. Ammonium persulfate decomposes in the solution to generate free radicals that initiate the polymerization reaction, while sodium bisulfite works synergistically with ammonium persulfate to stabilize the reaction and prevent side reactions.

3. Initiator Addition

Slowly add the initiator solution to the reaction system through a constant pressure dropping funnel. The addition rate must be precisely controlled to ensure a stable reaction rate. During the reaction, turn on the magnetic stirrer to ensure uniform mixing of the reactants and to avoid localized overheating or uneven reactions.

4. Heating and Polymerization Reaction

As initiator is added, gradually increase the temperature to the preset reaction temperature, typically 60–70 °C. This temperature range effectively promotes free radical generation and maintains smooth polymerization. During the reaction, nitrogen is continuously added to remove oxygen from the solution and prevent oxidation from inhibiting the free radical polymerization process.

5. Reaction Completion and Termination

The polymerization reaction lasts for a certain time (typically adjusted according to the characteristics of the reaction system), at which point the polymer has formed. The reaction is terminated by cooling the mixture to room temperature. This process can be further controlled by adding an appropriate terminator (such as diphenylmethane).

6. Product Treatment

Upon completion of the reaction, the reaction product must be removed from the flask and a purification procedure must be performed. First, the product must be washed with water to remove unreacted monomers, solvents, and initiators. Then, the product must be filtered through filter paper or a filtration membrane to remove solid contaminants. Finally, the product must be dried to remove moisture and residual solvents.

7. Grinding and Drying

The dried product is solid and granular and requires further processing through a grinder to produce fine, uniform polymer powder particles, called SH, for use in subsequent experiments or applications.

The reaction equation is as follows (Fig. 1):

Table 1. Composition of Cement (%)

SiO_2	Fe_2O_3	Al_2O_3	MgO	CaO	SO_3	K_2O	Na_2O
21.05	3.90	5.30	1.75	62.25	2.65	0.20	0.25

Table 2. Composition of Fly Ash (%)

SiO_2	Fe_2O_3	Al_2O_3	MgO	CaO	SO_3	K_2O	Na_2O
58.00	4.82	21.52	1.37	7.92	0.14	1.12	0.88

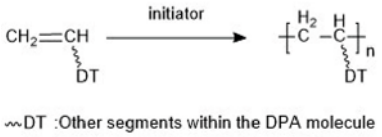

Figure 1. The reaction equation for SH

(2) Cement Paste Preparation

The cement and fly ash are weighed and mixed in a dry mixer for one minute. VAE is then added, and the dry mixing is continued for an additional minute. SH, SHMP, and EDTA-4Na are dissolved in a portion of water to prepare a solution, which is then mixed with the remaining water. The mixture is slowly added to the dry materials and stirred at low speed for two minutes. Following this, the machine should be stopped to scrape the walls, and the stirring should be continued at high speed for two minutes until the mixture has reached homogeneity. The mixture should then be poured into a cylindrical mold measuring 100 mm in diameter and 50 mm in height, and the mixture should be vibrated to compact. It is imperative to maintain a curing temperature of 25 ±5 °C and to ensure that the relative humidity is maintained at a minimum of 90%. After 24 hours, the mixture should be demolded, and tests for basic properties, permeability, etc., should be conducted.

(3) Crack Formation in Cement Paste

The apparatus consists of a pressure machine combined with a custom-made wedge knife, which is used to create cracks in the cement paste with a "V"-shaped fracture method. The crack width is precisely controlled by filling with metal fine wires[28], as illustrated in Figure 2.

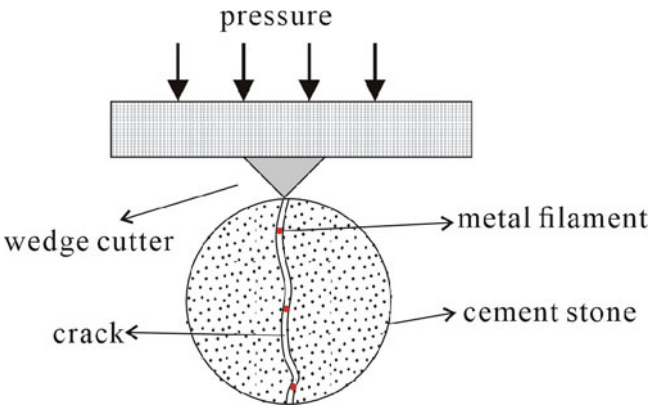

Figure 2. Schematic Diagram of Microcrack Formation in Cement Paste

(4) Cement Paste Curing Environment

A water solution with a pH of 7.85 and a $Ca(OH)_2$ solution with a saturation level and a pH of 12.53 were used as curing environments for the crack healing experiments. During the curing process, a wet-dry cycling method was applied, with each cycle lasting 24 hours. The environmental temperature was controlled at 25±5 °C, and the relative humidity was controlled at 80%±5%. The curing solution was replaced every 7 days to ensure the stability and accuracy of the experimental conditions.

Formulation Design and Selection

(1) Formulation Design

The base formulation for the cement paste includes a water-to-cement ratio of 0.35 and a fly ash content of 20% by mass relative to cement. Different dosages of complexing agents (SH, SHMP, EDTA-4Na) and VAE affect the properties of self-healing cementitious materials, making it necessary to conduct in-depth research to optimize the material formulation. Orthogonal experiments, which select representative experimental points based on orthogonality and study multiple factors and levels, allow for efficient and effective experimental conclusions to be drawn while reducing the number of trials[29]. In this experiment, a four-factor three-level orthogonal design was adopted, with the crack sealing rate after 28 days of curing as the evaluation index. A compression strength of less than 42.5 megapascals after 28 days of cure was used as an exclusion criterion. A comprehensive review of the extant literature has been conducted to ascertain the composition of the self-healing material and the levels of candidate factors[25, 26] .The results of these investigations are delineated in Table 3.

The orthogonal experiment design table is shown in Table 4.

Table 4. Orthogonal Experiment Table

No	SH (%)	SHMP (%)	EDTA-4Na (%)	VAE (%)
Test 1	Ⅰ	Ⅰ	Ⅰ	Ⅰ
Test 2	Ⅰ	Ⅱ	Ⅱ	Ⅱ
Test 3	Ⅰ	Ⅲ	Ⅲ	Ⅲ
Test 4	Ⅱ	Ⅰ	Ⅱ	Ⅲ
Test 5	Ⅱ	Ⅱ	Ⅲ	Ⅰ
Test 6	Ⅱ	Ⅲ	Ⅰ	Ⅱ
Test 7	Ⅲ	Ⅰ	Ⅲ	Ⅱ
Test 8	Ⅲ	Ⅱ	1	Ⅲ
Test 9	Ⅲ	Ⅲ	Ⅱ	Ⅰ

(2) Formulation Optimization

The experimental method for evaluating permeability is delineated in Section 2.4.2, and the findings of the experiment are exhibited in Table 5.

Based on the experimental findings, the average sealing rate for each factor at various levels was calculated, as

Table 3. Orthogonal Experiment Factor Level Table

Levels	Factors			
	SH (%)	SHMP (%)	EDTA-4Na (%)	VAE (%)
Ⅰ	0	0	1	1
Ⅱ	0.5	0.05	3	3
Ⅲ	1	0.1	5	5

Table 5. Compressive strength and permeability test results following 28 days of curing

No.	Ⅰ	Ⅱ	Ⅲ	Ⅳ	Ⅴ	Ⅵ	Ⅶ	Ⅷ	Ⅸ
Sealing Rate (%)	72.60	80.20	94.40	84.30	85.40	89.10	99.60	94.20	99.10
Compressive Strength (MPa)	37.32	44.51	42.83	46.36	51.93	47.81	43.67	45.60	49.60

presented in Table 6, while the changes in compressive strength are provided in Table 7.

The experimental results reveal that the factors impacting the sealing rate of the self-healing material, ranked by significance, are SH, SHMP, EDTA-4Na, and VAE. The key determinants of the self-healing material's strength, ranked by their impact, are SH, SHMP, EDTA-4Na, and VAE. Under the premise of ensuring a compressive strength ≥ 42.5 MPa, the optimized material formulation is as follows: SH accounts for 0.5% of the cement mass, SHMP accounts for 0.05% of the cement mass, EDTA-4Na accounts for 3% of the cement mass, and VAE accounts for 5% of the cement mass.

Experimental Methods

Based on the above formulation conclusions, the composite complexing agents were mixed in the ratio of SH: SHMP: EDTA-4Na: VAE = 10:1:60:100. Specimens were prepared with the composite complexing agent mass ratio to cement mass at 0%, 2%, 4%, and 6%, denoted as C0, C2, C4, and C6, respectively.

Structural Characterization

The FTIR analysis of the synthesized SH was conducted using the WQF-520 FTIR spectrometer model from Beijing Reilly Analytical Instrument Co., Ltd. The wavenumber range was 4400–400 cm^{1}, with 10 scans and a resolution error of 5 cm^{1}.

Basic Performance Characterization

Mercury Intrusion Porosimetry

The cement paste samples were meticulously trimmed into cubic blocks measuring precisely 1 centimeter. These samples were then subjected to a drying process in a desiccator, a controlled environment that facilitated the attainment of a constant weight. The distribution of pore sizes in the samples was measured using the Micromeritics AutoPore IV 9500 series automatic mercury intrusion porosimeter, supplied by Micromeritics (Shanghai) Instruments Co., Ltd. The test pressure range was from 0 to 414 MPa (60,000 psi). The test followed the ASTM D4404 standard, and the test temperature was 25 °C. It should be noted that the experimental process needs to be repeated to confirm whether the sample is damaged, damaged samples of the test results will not have the reliability, if necessary, can be considered for the sample to add a certain degree of protection to improve.

Thermal Analysis Test

Thermogravimetric analysis (TGA) was employed to investigate the impact of the composite complexing agent on the hydration process. The experiment was conducted using a NETZSCH STA449F3 thermogravimetric analyzer produced by NETZSCH, Germany. The degree of hydration was evaluated by calculating the content of chemically bound water for the cement--based material[30–32].

Self-healing Performance Characterization

Compressive Strength Test

To examine how various composite complexing agents influence the mechanical performance recovery of cement-based materials, compressive strength tests were conducted to assess their performance. The curing durations were established as 3, 7, 14, 21, and 28 days. The experiment was carried out using a WHY-1000 microcomputer-controlled fully automatic pressure testing machine. Four specimens were set for each mix ratio as a group. Based on the principle of data validity, data with deviations exceeding ±10% of the average value were discarded, and the final average compressive strength was calculated.

Table 6. Orthogonal Experiment Calculation Results of Sealing Rate

Factors	SH	SHMP	EDTA-4Na	VAE
Level1 (%)	82.40	85.50	85.30	85.70
Level2 (%)	86.27	86.60	87.87	89.63
Level3 (%)	97.63	94.20	93.13	90.97
Range (%)	15.23	8.70	7.83	5.27

Table 7. Orthogonal Experiment Calculation Results of Compressive Strength

Factors	SH	SHMP	EDTA-4Na	VAE
Level1 (MPa)	41.55	42.45	43.58	46.28
Level2 (MPa)	48.70	47.35	46.82	45.33
Level3 (MPa)	46.29	46.75	46.14	44.93
Range (MPa)	7.15	4.90	3.25	1.35

Permeability Evaluation

The efficacy of crack self-repairing was assessed by comparing the permeability of cement paste cracks before and after healing. The cement paste samples with cracks were fixed in metal sleeves using resin to ensure that water only leaked through the cracks at the ends of the cement paste specimens. The water penetration through the cement paste was measured for 1 minute at various time intervals, specifically on days 3, 7, 14, 21, and 28, and the sealing rate of the cracks in the cement paste was calculated using formulas (1). In an effort to eradicate human error, a total of five sets of specimens were meticulously selected for each mix ratio. The final experimental results were then calculated as the average of these five sets, thereby ensuring the most accurate and reliable outcomes. The crack sealing rate of cement paste micro-cracks is calculated using formula (1).

$$E = \frac{K_{\text{initial}} - K_{\text{curing n days}}}{K_{\text{initial}}} \times 100\% \quad (1)$$

Where:

E – Crack sealing rate

K_{initial} – Initial permeability, μm².

$K_{\text{curing n days}}$ – The permeability after self – healing for n days, μm².

XRD

The cement paste crack self-healing material samples were oven-dried, followed by grinding into a fine powder. This powder was then sifted through a 60 mesh sieve to prepare the samples for XRD testing. Then, the products of the cement paste were analyzed using an XRD instrument (X'Pert MPD PRO, Netherlands).

RESULTS AND ANALYSIS

Structural Characterization

By comparing and analyzing the infrared spectra in Figure 3, several key features can be observed:

First, in the high-frequency region, the absorption bands at 3325 cm⁻¹ and 3320 cm⁻¹ correspond to the characteristic stretching vibrations of hydroxyl groups (-OH). In the mid-frequency region, the strong absorption peaks at 1646 cm⁻¹ and 1645 cm⁻¹ represent the stretching vibrations of the carbonyl group (C=O) in the amide group. In the fingerprint region, the peaks at 992 cm⁻¹ and 915 cm⁻¹ are typical of the out-of-plane bending vibrations of the C-H bonds in mono-substituted alkenes.

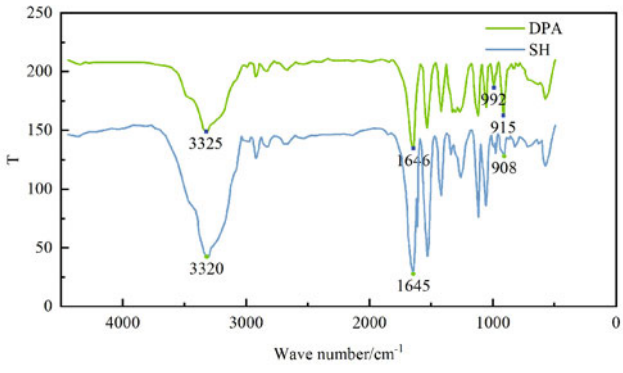

Figure 3. Infrared Spectra of DPA and SH

A comparison of the spectra of SH and DPA reveals two significant changes. Firstly, the out-of-plane bending vibration peak of the C-H bond in mono-substituted alkenes at 992 cm⁻¹, which was originally present in the SH spectrum, completely disappears. Secondly, the absorption intensity of the -OH stretching vibration peak and the amide C=O stretching vibration peak in SH is significantly enhanced.

These spectral changes confirm that DPA has undergone a successful polymerization reaction, resulting in the target product, SH. The disappearance of the characteristic peak at 992 cm⁻¹ directly reflects the involvement and transformation of the olefinic group during the polymerization process.

Basic Performance Characterization

Mercury Intrusion Porosimetry Analysis

Following the confirmation that the samples had not been damaged, the test results were plotted in Figure 4. As demonstrated in Figure 4(a), significant differences were observed in the pore size distribution and cumulative intrusion volume among the samples. The C0 sample exhibited a pronounced peak in the macropore range (>10³ nm), indicating the presence of more macroporous structures. As the proportion of the composite complexing agent (C0 → C6) increases, the peak in the macropore range gradually diminishes, while the peak in the mesopore and micropore range (<10² nm) progressively strengthens, particularly notable

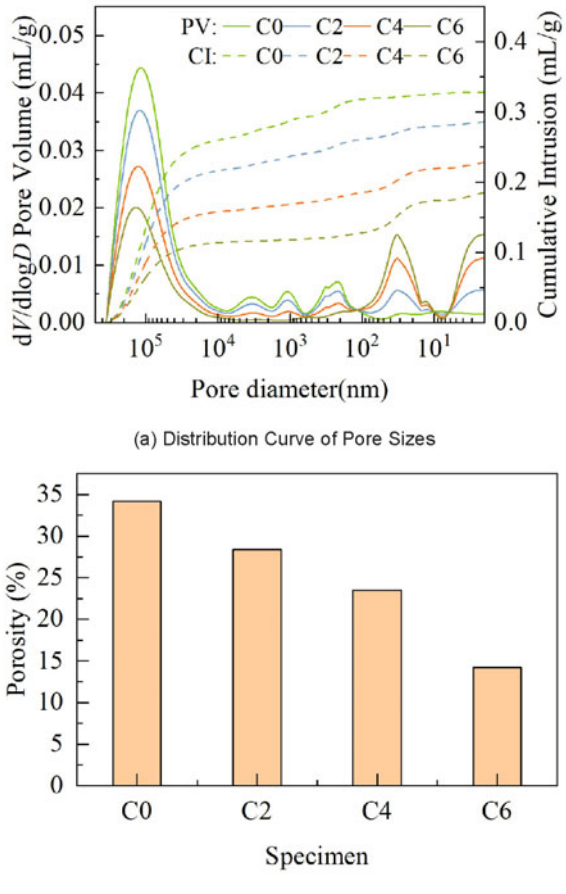

Figure 4. Mercury Intrusion Test Results for Cement Stones with Varying Quantities of Composite complexing Agents

in the C4 and C6 samples. These results indicate that incorporating the composite complexing agent facilitates the gradual occupation of macropores and promotes the development of additional mesoporous and microporous structures.

Furthermore, the cumulative intrusion volume exhibits a decrease from 0.4 mL/g for C0 to 0.15 mL/g for C6, indicative of a substantial reduction in total pore volume with increasing amounts of the composite complexing agent. Additionally, a shift in the pore size distribution towards smaller pores is observed. This phenomenon further corroborates the hypothesis that the composite complexing agent exerts a profound effect on the reorganization and densification of the pore structure. Additionally, there is an increase in the proportion of non-harmful pores (≤20 nm) and a concomitant decrease in the proportion of detrimental pores (>200 nm). This results in a substantial enhancement of the material's mechanical properties[33].

As illustrated in Figure 4(b), the porosity of the samples exhibits a clear trend of decreasing porosity with increasing composite complexing agent concentration. The C0 sample has the highest porosity at 34.2%, while the C6 sample has the lowest porosity of 14.2%, which is more than half of the initial value. This indicates a substantial decrease in porosity with increasing composite complexing agent concentration. This decrease is closely related to the compaction and closure effects of the pore structure. This trend is consistent with the observed changes in cumulative intrusion volume, thereby confirming the intrinsic relationship between reduced porosity and material densification.

The alterations in the pore size distribution are primarily attributable to the crystal precipitation that ensues from the incorporation of the complexing agent, which serves to fill the original pores. As illustrated in Figure 5, the decline in the proportion of large particles and the rise in small particles in cement result in a substantial enhancement of inter-particle rearrangement and the generation of cementation products. This process effectively fills the original pores, thereby leading to the densification and reduction in porosity of the material.

Figure 6 presents the TG/DTG curves at 3 days and 28 days of hydration. By comparing these curves, the following observations can be made:

(1) Early Hydration Stage (3 days)

In the 50–200 °C range, an increase in the content of the composite complexing agent (C0 → C6) is accompanied by a gradual decrease in mass loss. This phenomenon indicates a reduction in the content of C-S-H gel and ettringite[34]. The underlying mechanism of this effect is attributed to the ability of complexing agents such as SH, SHMP, and EDTA-4Na to form stable complexes with Ca^{2+}, thereby inhibiting the early hydration reactions.

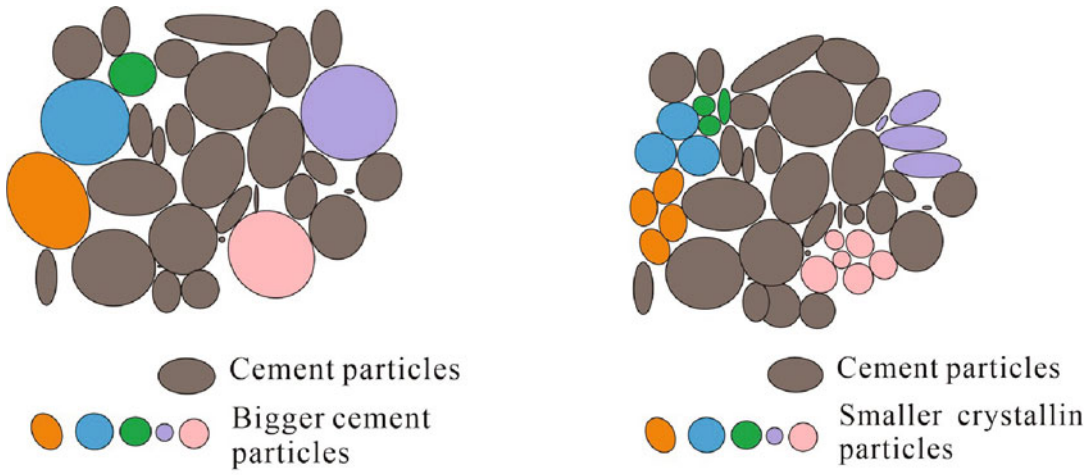

(a) Pore Distribution in C0 (b) Pore Distribution in C6

Figure 5. Mechanism Diagram of Pore Distribution Changes

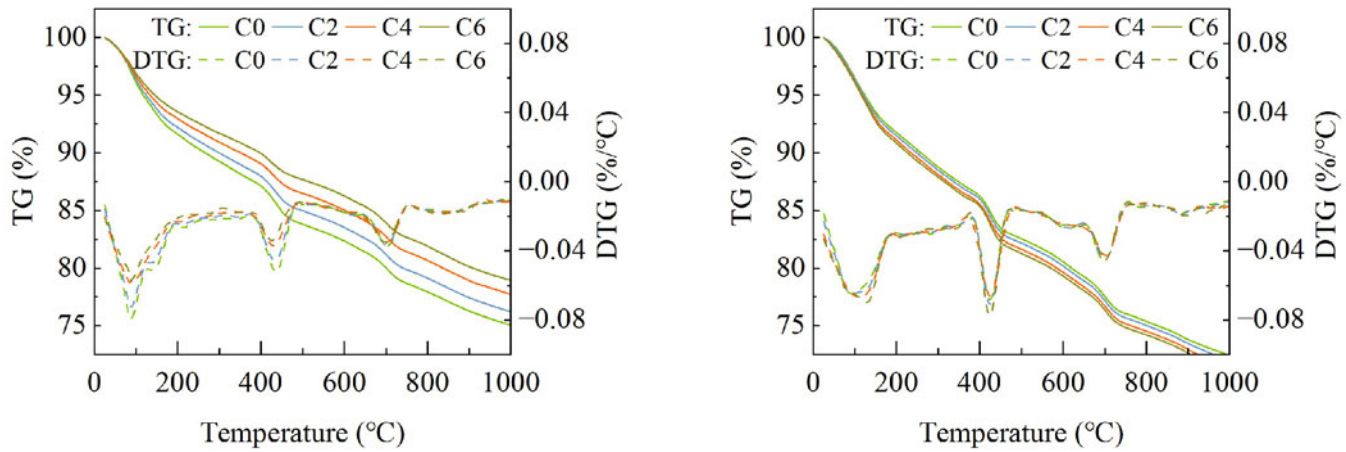

(a) 3d (b) 28d

Figure 6. TG/DTG Curves of Different Contents of Composite Complexing Agents at Various Hydration Stages

In the 420–470 °C range, the DTG curve shows a weakening of the $Ca(OH)_2$ decomposition peak[35] as the amount of composite complexing agent increases, suggesting a decrease in the content of $Ca(OH)_2$ in the early hydration products.

In the 660–740 °C range, corresponding to the decomposition of $CaCO_2$[36] the mass loss decreases as the composite complexing agent content increases. It has been demonstrated that incorporating the composite complexing agent results in a decrease in the early carbonation degree.

The C6 sample shows the least mass loss across all temperature ranges, indicating that the high dosage of the composite complexing agent most significantly inhibits early hydration.

(2) Later Hydration Stage (28 days)

The discrepancy in mass loss within the 50–200 °C range becomes less pronounced, and as the composite complexing agent content increases (C0 → C6), the mass loss gradually rises, indicating that, as the curing time progresses, the previously suppressed hydration reactions gradually recover, and the incorporation of the composite complexing agent enhances the hydration degree of the samples to a certain extent.

The variation in the $Ca(OH)_2$ decomposition peak within the 420–470 °C range exhibits a decline, indicating that the generation of $Ca(OH)_2$ in subsequent stages approaches a state of equilibrium.

In the 660–740 °C range, the decomposition of $CaCO_3$ becomes more consistent, indicating minimal differences in carbonation degree among the samples in the later stage. This phenomenon is attributed to the densification structure that is governed by the composite complexing agent.

The TG curves from C0 to C6 show a more consistent trend, indicating that, after 28 days, the differences in the hydration degree of the samples become smaller.

The influence of the composite complexing agent on hydration is observed to shift from significant inhibition to mild enhancement over the course of a period ranging from three days to 28 days. This change suggests that the effect of the complexing agent is time-dependent: initially, it temporarily inhibits hydration by complexing with Ca^{2+}, and then, as the complexes gradually decompose, they release Ca^{2+} to promote continued hydration.

This hydration process regulation mechanism corresponds to the previously mentioned evolution of pore structure: early hydration inhibition helps reduce the disorderly growth of hydration products, while slow hydration in the later stages contributes to the formation of a more compact microstructure.

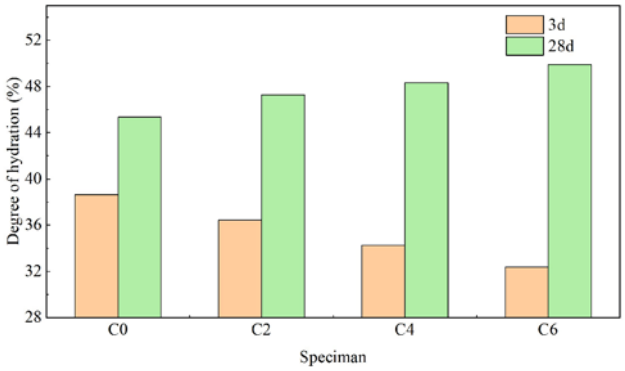

Figure 7. Hydration Degree of Self-Healing Materials Containing Different Composite Complexing Agents

As shown in Figure 7, the hydration degree of cement-based materials containing different composite complexing agents was investigated using the chemical combined water method for specimens with different curing ages. During the preliminary setting phase, which lasted for a period of three days, the incorporation of composite complexing agents led to a substantial decrease in the hydration level of the materials. Specifically, compared to the control group C0, the hydration degrees of specimens C2, C4, and C6 were reduced by 5.6%, 11.3%, and 16.3%, respectively. This indicates that with the increasing content of composite complexing agents, their inhibitory effect on hydration degree gradually strengthens. This phenomenon occurs because, during the initial hydration process, composite complexing agents form calcium complexes, which impede the dissolution of cement minerals and decrease the concentration of Ca^{2+} in the liquid phase. Consequently, this hinders the hydration reaction.

However, in the later curing stage (28 days), the effect of composite complexing agents on hydration degree shows the opposite trend. As the curing age extends, the hydration degrees of specimens C2, C4, and C6 increase by 4.2%, 6.5%, and 10.0%, respectively, compared to the control group C0. This phenomenon indicates that, although there was an inhibitory effect initially, over time, the calcium complexes, transported by water, move and expose the unhydrated cement particles they encapsulate to water, allowing continued hydration. Additionally, the complexation-substitution reactions between the complexing agents and calcium ions may have also promoted the hydration process in the later stage.

Self-Healing Performance Characterization

Compressive Strength Evaluation

As demonstrated in Figure 8, in the initial healing phase (3 days), specimens containing composite complexing agents exhibit a conspicuously elevated compressive strength recovery rate in comparison to the C0. Specifically, after 3 days of healing in water, the compressive strength of C0 reaches 63.4% of its 28-day strength, while specimens C2, C4, and C6 with different doses of composite complexing agents achieve 65.8%, 66.3%, and 68.0% of their respective 28-day strengths. This finding suggests that the incorporation of the composite complexing agent enhances the recovery of early mechanical properties in cement stone, with the acceleration effect becoming more pronounced at higher dosages.

The curing environment has a significant impact on the composite complexing agent's promotion of self-healing. Following a 28-day water-curing process, the compressive strengths of specimens C0, C2, C4, and C6 were recorded as 41.3 MPa, 45.5 MPa, 48.1 MPa, and 49.6 MPa, respectively. However, after a 28-day period of curing in a calcium hydroxide solution, the corresponding compressive strength values increase to 47.5 MPa, 52.3 MPa, 55.2 MPa, and 56.0 MPa, which are 17.8%, 16.9%, 13.9%, and 15.1% higher than those

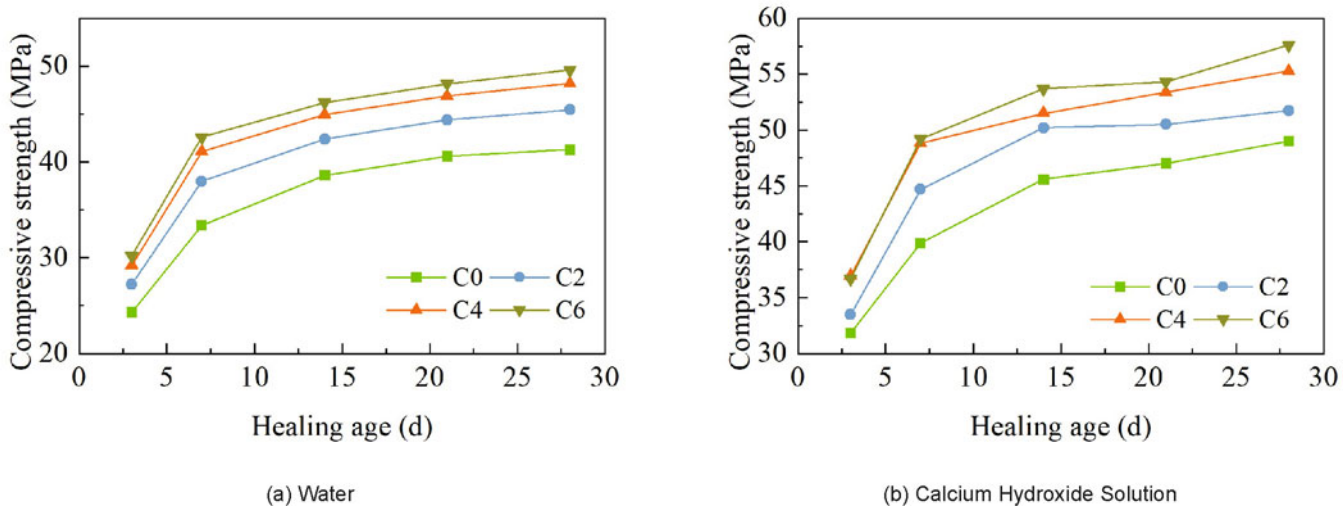

Figure 8. Compressive Strength During the Healing Process in Different Curing Environments

in the water curing environment. This phenomenon suggests that the Ca^{2+}-rich alkaline environment promotes the activation mechanism of the composite complexing agent, thereby enhancing the self-repairing effect of cementitious materials.

Permeability Evaluation

As illustrated in Figure 9, the impact of the composite complexing agent on the crack sealing rate of cement--based materials tested in two distinct environments, water (a) and calcium hydroxide saturated solution (b), is examined. The findings suggest that the incorporation of the composite complexing agent significantly enhances the crack self-repairing capacity of materials. Meanwhile, the experimental results show that, whether in aqueous solution or in saturated calcium hydroxide solution, as the self - healing time progresses, the self – healing rate of cracks exhibits an upward trend. Moreover, with the increase in the dosage of the composite complexing agent, there is a tendency for the self-repairing rate to increase.

In the water curing environment, the sealing rate of cracks in the control group C0 increased from approximately 31.5% at 3 days to about 73.1% at 28 days. In contrast, the sealing rates of specimens C2, C4, and C6 with the composite complexing agent increased from 35.5%, 38.2%, and 39.5% at 3 days to 86.4%, 95.3%, and 99.7%, respectively, at 28 days. This indicates that the presence of the composite complexing agent not only improves the early healing rate but also significantly enhances the final sealing effect.

In the calcium hydroxide saturated solution curing environment, all specimens exhibited enhanced crack sealing performance, with the sealing rate of cracks in the control group C0 increasing from approximately 38.5% at 3 days to approximately 81.6% at 28 days. For specimens C2, C4, and C6, the sealing rates increased from 43.1%, 46.1%, and 47.6% at 3 days to 90.7%, 96.8%, and 99.8%, respectively, at 28 days. This outcome suggests that the calcium-rich alkaline environment further enhances the efficacy of the composite complexing agent, resulting in accelerated early healing rates and elevated final sealing rates. It is noteworthy that the C6 specimen exhibited the most optimal performance in the calcium hydroxide solution, achieving a sealing rate of 99.8% at 28 days. This outcome fully validates the exceptional self-healing capabilities of the composite complexing agent under conducive conditions.

XRD Analysis

As illustrated in Figure 10(a), the characteristic peaks of $Ca(OH)_2$ (2θ = 18.0°, 28.6°, 34.0°, 47.0°) undergo a gradual decrease in intensity with increasing content of the complexing agent. This observation indicates that the complexing agent accelerates the consumption of

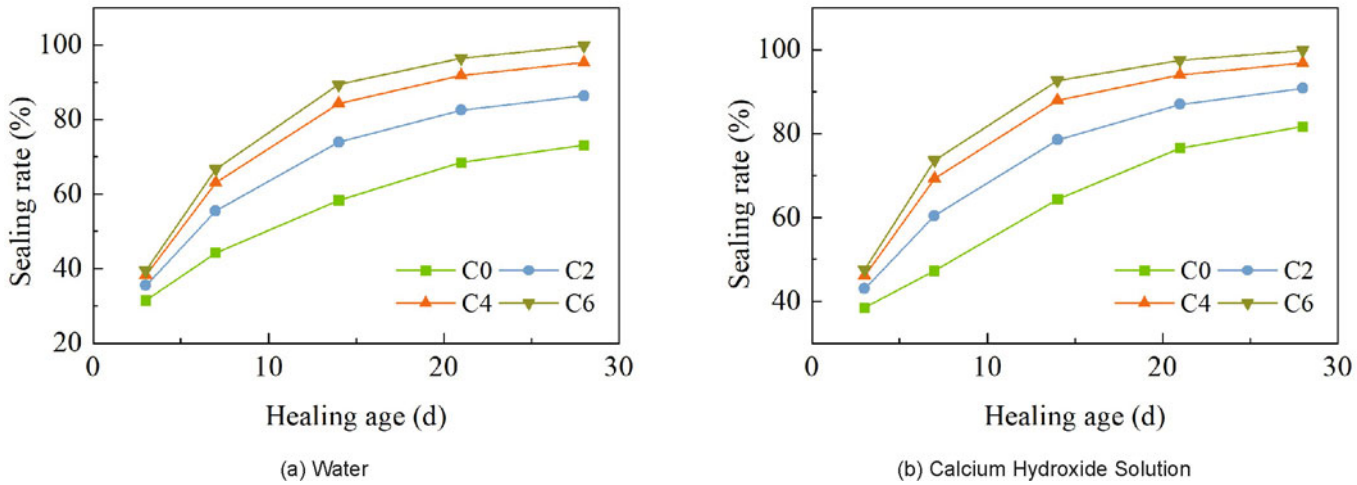

Figure 9. Sealing Rate During the Healing Process in Different Curing Environments

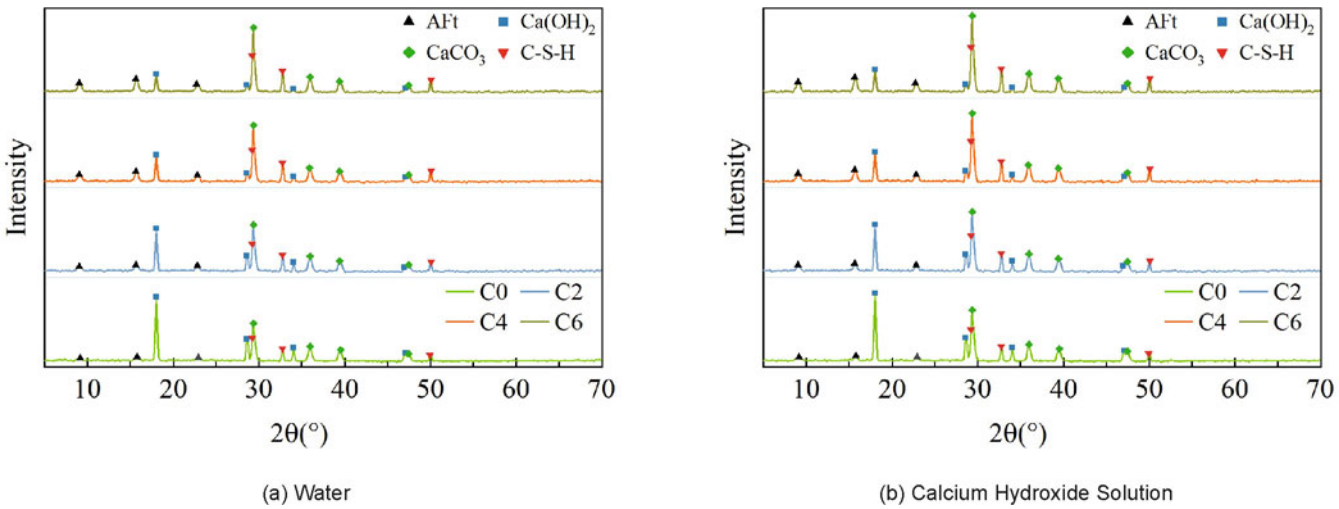

Figure 10. XRD Diffractograms of Self-Healing Products from Cracks After 28 Days of Curing in Different Environments

$Ca(OH)_2$. Concurrently, the peak intensity of $CaCO_3$ (2θ = 29.4°, 36.0°, 39.5°, 47.5°) exhibited an increase with the addition of the complexing agent, reaching its maximum at the C6 specimen. This observation indicates that the complexing agent facilitates the reaction between Ca^{2+} and CO_3^{2-} in water, leading to an enhanced formation of $CaCO_3$. In accordance with the findings reported in relevant literature[37], the predominant phase of CSH(PEG-0) was identified as Jennite (PDF card 18–1206, chemical formula $Ca_9Si_6O_{18}(OH)_6 \cdot 8H_2O$). The diffraction reflections were located at 8.40°, 29.92°, 31.78°, 35.74°, and 49.70°, respectively. The peak intensities of C-S-H (2θ = 29.3°, 31.8°, 50.0°) and AFt (2θ = 9.1°, 15.7°, 22.8°)[38] also increased with the content of the complexing agent, further indicating that the complexing agent promoted the hydration of the cement matrix, enhancing the material's densification and crack repair capacity.

By comparing Figure 10(a) and 10(b), it is evident that the amount of $CaCO_3$ generated in the calcium hydroxide saturated solution is significantly higher than in the water curing environment. The elevated concentration of calcium ions within the solution is the primary factor contributing to this phenomenon, as it facilitates more efficient complexation reactions. Overall, the crack repair effect under the calcium hydroxide saturated solution curing environment is much better than that under water curing.

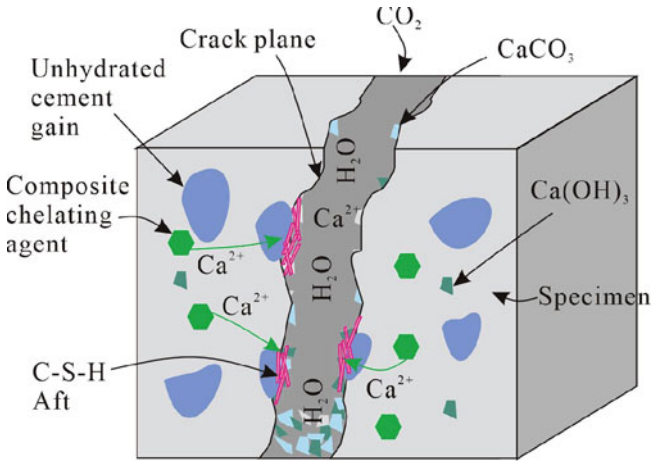

Figure 11. Schematic Diagram of the Self-Healing Mechanism of Cement Stone Cracks

As demonstrated in Figure 11, the mechanism of the composite complexing agent in crack repair of cement--based materials primarily involves a complexation--precipitation reaction. The active components of the composite complexing agent react with Ca^{2+} to form complexes, consuming a significant amount of $Ca(OH)_2$ and producing unstable complexes. These complexes further transform into stable $CaCO_2$, C-S-H, and AFt precipitates, which fill cracks and pores, enhancing the material's densification and strength. Particularly in the calcium hydroxide saturated solution, the abundant Ca^{2+} provides a sufficient calcium source for the complexation reaction, significantly accelerating the consumption of $Ca(OH)_2$ and the formation of $CaCO_2$, thus improving the self-healing effect.

In the context of water-curing environments, the reduced concentration of Ca^{2+} ions leads to constrained complexation reactions and the subsequent formation of self-healing products, consequently yielding diminished crack repair efficacy. Conversely, the calcium hydroxide saturated solution offers a heightened concentration of Ca^{2+} ions, enabling more comprehensive complexation reactions and the generation of additional self-healing products (e.g., $CaCO_3$, C-S-H, and AFt), thereby markedly enhancing the crack repair outcome.

Furthermore, the composite complexing agent has been shown to promote the ongoing hydration of unhydrated cement particles. This process results in the formation of more C-S-H and AFt. This phenomenon not only facilitates crack repair but also contributes to the enhancement of the material's compressive strength and durability. This mechanism provides a theoretical foundation for the utilization of composite complexing agents in cement-based materials.

CONCLUSION

The findings indicate that self-healing cementitious materials based on the composite complexing agent demonstrate remarkable hydration performance, pore structure optimization, and crack self-healing capabilities. This study offers novel insights and theoretical underpinnings that provide a foundation for the design and development of self-healing cement stone materials. The conclusions were as follows:

(1) Through orthogonal experiments, the optimal mixture ratio of the composite complexing agent was determined as follows: SH accounts for 0.5% of the cement mass, SHMP for 0.05%, EDTA-4Na for 3%, and VAE for 5% of the cement mass.

(2) The composite complexing agent significantly improved the pore characteristics of cement stone. When the amount of composite complexing agent was 6% of the cement mass, the porosity of cement stone decreased from 34.2% to 14.2%, and larger pores were converted to smaller ones, greatly enhancing the material's density and improving the overall performance of the cement stone.

(3) The composite complexing agent demonstrated a marked reduction in the early (3-day) hydration degree of cement stone. Specifically, the hydration degree of samples containing 6% of the agent was found to be 16.3% lower than that of the control group. However, the composite complexing agent significantly enhanced the hydration degree of cement stone in the later stage (28 days and beyond). Specifically, samples with the composite complexing agent exhibited a 10% higher hydration degree compared to the control group.

(4) The composite complexing agent effectively achieved crack self-healing. Following a 28-day period of water curing, the compressive strength of the specimen containing a 6% composite complexing agent exhibited an increase of 8.3 megapascals (MPa) in comparison with the control group. Concurrently, the crack sealing rate demonstrated a notable rise, increasing from 73.1% to 99.7%. Additionally, the self-healing performance in calcium hydroxide saturated solution exhibited superiority over that in water curing environment.

(5) XRD analysis indicated that the primary healing products in the cracks were $CaCO_3$ and C-S-H, followed by AFt and a small amount of $Ca(OH)_2$. The composite complexing agent effectively combined with Ca^{2+} and released it during the curing process of cement stone cracks, reacting with CO_3^{2-} and unhydrated cement particles to form the healing materials.

The effects of long-term environmental factors (e.g., temperature and humidity alternation, chemical attack) were not considered in this study, and the self-healing stability of the composite fitters under complex stress conditions was not verified. In the future, it is necessary to combine accelerated aging tests with multi-axial loading experiments to optimize the material formulations and explore the potential for engineering applications.

Funding: This work was supported by the Chongqing Talent Program Project (cstc2024ycjh-bgzxm0141).

LITERATURE CITED

1. Mignon, A., Snoeck, D., Dubruel, P., Van Vlierberghe, S. & De Belie, N. (2017). Crack mitigation in concrete: Superabsorbent polymers as key to success? *Materials*, 10(3), 237. DOI: 10.3390/ma10030237.

2. Yunovich, M. & Thompson, N.G. (2003). Corrosion of highway bridges: Economic impact and control methodologies. *Concr. Int*., 25(1), 52–57.

3. Bettigole, N. (1994). Rebuilding our bridges--why and how. ASTM Standardization News, 22(7).

4. Xincheng, P. (2012). Super-high-strength high performance concrete. CRC Press.

5. Dehwah, H.A.F. (1990). Durability of reinforced concrete beams repaired with various repair materials. King Fahd University of Petroleum and Minerals (Saudi Arabia).

6. Lin, X., Li, W., Castel, A., Kim, T., Huang, Y., Wang, K. (2023). A comprehensive review on self-healing cementitious composites with crystalline admixtures: Design, performance and application. *Constr. Build. Mater*., 409, 134108. DOI: 10.1016/j.conbuildmat.2023.134108.

7. Gruber, D., Ruiz-Agudo, C., Rao, A., Pasler, S., Cölfen, H. & Sturm, E.V. (2024). Complex coacervates: From polyelectrolyte solutions to multifunctional hydrogels for bioinspired crystallization. *Crystals*, 14(11), 959. DOI: 10.3390/cryst14110959.

8. Fernandes, J.F., Futai, M.M., Figueiredo, A.D.D. & Aoki, I.V. (2024). Non-destructive tests for performance evaluation of self-healing concrete by addition of methyl methacrylate--containing microcapsules. Revista IBRACON de Estruturas e Materiais, 17(2), 1–14. DOI: 10.1590/S1983-41952024000200006.

9. Huang, H. & Ye, G. (2012). Simulation of self-healing by further hydration in cementitious materials. Cem. Concr. Compos., 34(4), 460–467. DOI: 10.1016/j.cemconcomp.2012.01.003.

10. Rule, J.D., Sottos, N.R. & White, S.R. (2007). Effect of microcapsule size on the performance of self-healing polymers. Polymer, 48(12), 3520–3529. DOI: 10.1016/j.polymer.2007.04.008.

11. Yang, S., Zhang, S. & Niu, L. (2024). Influence of superabsorbent polymers on self-healing of cement-based materials containing magnesium oxide expansive agents. *Ind. Eng. Chem. Res.*, 63(34), 15151–15164. DOI: 10.1021/acs.iecr.4c02118.

12. Li, J., Bai, S. & Guan, X. (2024). Development optimization and performance evaluation of mineral capsules based on magnesium oxide expansive agent. *J. Build. Eng.*, 86, 108825. DOI: 10.1016/j.jobe.2024.108825.

13. Liu, Y., Zhou, L., Wan, X., Tang , Y., Liu, Q., Li, W. & Liao, J. (2024). Synthesis and Characterization of a Temperature-Sensitive Microcapsule Gelling Agent for High-Temperature Acid Release. ACS omega, 9(19), 20849–20858. DOI: 10.1021/acsomega.3c09586.

14. Qian, H., Umar, M., Nasir Ayaz Khan, M., Shi, Y., Manan, A., Raza, A., Li, F., Li, Z. & Chen, G. (2024). A state-of-the-art review on shape memory alloys (sma) in concrete: Mechanical properties, self-healing capabilities, and hybrid composite fabrication. *Mater. Today Commun*., 40, 109738. DOI: 10.1016/j.mtcomm.2024.109738.

15. Xu, R., Liao, L., Liang, W., Wang, H., Zhou, Q., Liu, W., Chen, M., Fang, B., Wu, D., Jin, H., Li, Y., Zou, S. & Lu, L. (2025). Fast Removing Ligands from Platinum-Based Nanocatalysts by a Square-Wave Potential Strategy. Angew. Chem. Int. Ed. Engl., 5, e202509746. DOI: 10.1002/anie.202509746.

16. Sun, Y., Wang, D., Wang, Z., Han, Z., Zhang, H., Ma, S. & Kong, X. (2024). Preparation and experimental study of corrosion-induced shape-memory fibers for crack repair. *Constr. Build. Mater.*, 457, 139349. DOI: 10.1016/j.conbuildmat.2024.139349.

17. Torkian, P., Baseri, H. & Karevan, M. (2024). Thermomechanical performance of polyester-based composites reinforced with polypropylene microfibers and carbon black nanoparticles. *J. Mater. Engin. Perfor.*, 1-20. DOI: 10.1007/s11665-024-10335-7.

18. Ghazouani, N., Raza, A. & Elhag, A.B. (2025). Synergistic effects of sma fibers and fly ash on the material characterization of recycled aggregate concrete. *Materials Letters,* 379, 137670. DOI: 10.1016/j.matlet.2024.137670.

19. Qian, C., Ren, L. & Luo, M. (2015). Development of concrete surface defects and cracks repair technology based on microbial-induced mineralization. *J. Chin. Ceramic Soc.*, 43, 619–631.

20. Talaiekhozani, A., Keyvanfar, A., Andalib, R., Samadi, M., Shafaghat, A., Kamyab, H., Abd Majid, M., Zin, R.M., Fulazzaky, M.A. & Lee, C.T. (2014). Application of proteus mirabilis and proteus vulgaris mixture to design self-healing

concrete. *Desalin. Water Treat.,* 52(19–21), 3623–3630. DOI: 10.1080/19443994.2013.854092.

21. Wang, R., Yu, J., Gu, S., He, P., Han, X. & Liu, Q. (2020). Investigation of self-healing capability on surface and internal cracks of cement mortar with ion chelator. *Constr. Build. Mater.*, 236, 117598. DOI: 10.1016/j.conbuildmat.2019.117598.

22. Wang, R., Yu, J., Liu, Q., Kuang, D. & Qiu, H. (2023). Synergistic effect of ion chelating agent and magnesium fluorosilicate on self-repairing ability and microstructure of mortar. *Constr. Build. Mater.*, 383, 131375. DOI: 10.1016/j.conbuildmat.2023.131375.

23. Zeng, C. (2007). Preparation and performance study of cement-based crystalline waterproofing agent (Master, Chongqing University).

24. Ren, Q., Wang, Q., Wu, Z., Liu, J., Xu, H.-Q., Wang, A., Zhang, X., Zhang, Z. & Ding, Y. (2024). Research on the properties of crystalline admixtures: Self-healing healing materials for concrete from multiple perspectives. *Constr. Build. Mate*r., 453, 139047. DOI: 10.1016/j.conbuildmat.2024.139047.

25. Zhang, C. (2022). Study on the self-healing performance of cementitious materials based on ion chelating agents (Ph.D, Harbin Institute of Technology).

26. Xia, X. (2022). Research on water self-healing agents for microcracks in oil well cement stone (Master, SouthWest Petroleum University).

27. Zhang, C., Ye, J., Liu, C., Guan, X., Li, J., Chen, X. & Yuan, J. (2024). Influence of various ion chelators on mechanical, transport and microstructure properties of cement-based materials. *Case Stud. Constr. Mater*., 21, e03709. DOI: 10.1016/j.cscm.2024.e03709.

28. Peng, Z., Xia, X., Feng, Q., Zheng, Y., Yu, C., Yang, Q. & Liu, X. (2022). Performance of permeable crystalline self-healing agent onmicro-cracks of oil well cement. *Arab. J. Sci. Eng.,* 47(5), 6073–6084. DOI: 10.1016/j.conbuildmat.2024.139047.

29. Wu, C.J. & Hamada, M.S. (2011). Experiments: Planning, analysis, and optimization. John Wiley & Sons.

30. Li, J., Wen, M., Yang, J., Liu, Y., Jiang, Z. & Chen, J. (2024). Synthesis and analysis of magnetic nanoparticles within foam matrix for foam drainage gas production. *Geoenergy Sci. Eng*., 238, 212887. DOI: 10.1016/j.geoen.2024.212887.

31. Ye, G., Liu, X., De Schutter, G., Poppe, A.M. & Taerwe, L. (2007). Influence of limestone powder used as filler in scc on hydration and microstructure of cement pastes. *Cem. Concr. Compos.*, 29(2), 94–102. DOI: 10.1016/j.cemconcomp.2006.09.003.

32. Li, J., Wen, M., Jiang, Z., Xian, L., Liu, J. & Chen, J. (2025). Development and characterization of a surfactant responsive to redox conditions for gas recovery in foam drainage. *Sci. Rep.,* 15(1). DOI: 10.1038/s41598-024-84256-9.

33. Wang, Y. (2001). Study on the composition, structure, shrinkage, and compensation of ultra-high-strength and high--performance concrete (Master, Chongqing University).

34. Lothenbach, B., Le Saout, G., Haha, M.B., Figi, R. & Wieland, E. (2012). Hydration of a low-alkali cem iii/b–sio2 cement (lac). *Cement and Concrete Res.*, 42(2), 410–423. DOI: 10.1016/j.cemconres.2011.11.008.

35. El-Diadamony, H., Amer, A.A., Sokkary, T.M. & El-Hoseny, S. (2018). Hydration and characteristics of metakaolin pozzolanic cement pastes. HBRC Journal, 14(2), 150–158. DOI: 10.1016/j.hbrcj.2015.05.005.

36. Pane, I. & Hansen, W. (2005). Investigation of blended cement hydration by isothermal calorimetry and thermal analysis. *Cement and Concrete Res*., 35(6), 1155–1164. DOI: 10.1016/j.cemconres.2004.10.027.

37. Guan, W., Ji, F., Chen, Q., Yan, P. & Pei, L. (2013). Synthesis and enhanced phosphate recovery property of porous calcium silicate hydrate using polyethyleneglycol as pore-generation agent. *Materials*, 6(7), 2846–2861. DOI: 10.3390/ma6072846.

38. Tchekwagep Jean Jacques, K., Fengzhen, Y., Shoude, W., Piqi, Z., Shifeng, H. & Xin, C. (2023). Analysis of the phases and functions of the various compounds of calcium sulfoaluminate cement after exposure to high temperature. *J. Mater. Res. Technol*., 25, 4154–4170. DOI: 10.1016/j.jmrt.2023.06.215.